Chapter 9
Characteristics of X-Ray Attenuation in Electrospun Bismuth Oxide/Poly-lactic Acid Nanofibre Mats

Abstract The characteristics of X-ray transmission in electrospun nano(n)- and micro(m)-Bi_2O_3/poly lactic acid (PLA) nanofibre mats with different Bi_2O_3 loadings were compared using mammography (22–49 kV) and X-ray absorption spectroscopy (XAS) (7–20 keV). Results indicate that X-ray transmissions by electrospun m-Bi_2O_3/PLA nanofibre mats are distinctly higher than those of n-Bi_2O_3/PLA nanofibre mats at all energies investigated. In addition, with increasing the filler loading (n-Bi_2O_3 or m-Bi_2O_3), the porosity of electrospun Bi_2O_3/PLA nanofibre mats decreased thus decreasing the X-ray transmission except for the nanofibre mat containing 38 wt% of Bi_2O_3 (the highest loading in the present study). The latter showed higher porosity with some beads formed thus resulting in a sudden increase in X-ray transmission.

9.1 Introduction

Nanoparticles, i.e. nanometric sized particles, have attracted much attention amongst researchers in different fields of physics, chemistry, material science, medicine, and biology, because of their unique and often superior electronic, magnetic, optical, mechanical, physical and chemical properties [1–7]. For example, in the medical field, nanoparticles have been widely used in diagnosis, tissue engineering and also as drug delivery devices [8]. Gold nanoparticles are one of the most useful nanoparticles in industry and medicine [3]. For instance, in the medical field, gold nanoparticles show significant improvement in the treatment of cancers by enhancing the sensitivity of radiation from a radiotherapy unit with minimal adverse effects on surrounding normal tissues [1, 2].

Additionally, this size-effect has also become one of the virtues in designing materials for shielding of ionizing radiations. Some X-ray technologists believe that this effect will improve the X-ray attenuation ability of the composite since nano-sized fillers are able to be dispersed more uniformly within the matrix with fewer agglomerations as compared to micro-sized fillers [9, 10]. The latest work done by Buyuk et al. [11] proved that decreasing the titanium diboride particle size in the titanium diboride reinforced boron carbide-silicon carbide composites causes

I. M. Low and N. Z. Noor Azman, *Polymer Composites and Nanocomposites for X-Rays Shielding*, Composites Science and Technology,
https://doi.org/10.1007/978-981-13-9810-0_9

higher linear attenuation coefficient values for the energy of 0.662 MeV emitted by Cs-137 gamma source [11] found that the nanostructured copper oxide (CuO) is more effective in attenuation of lower X-ray beam energy (26 and 30 kV) and no significant variation in X-ray attenuation at higher X-ray beam energy (60 and 102 kV). Künzel and Okuno [12] also provided similar results, which show that the X-ray absorption is higher for a nanostructured CuO compound compared to the microstructured counterpart for low energy X-ray beams (25 and 30 kV) for all CuO concentrations incorporated into polymeric resins.

Electrospinning is a well-established polymer processing technique which has been proven to be a flexible and effective method for fabricating multilayers of microscale (>1 μm) to the nanoscale (<1000 nm) fibres from different types of polymers to be used in a wide range of applications such as in drug delivery, tissue engineering and protective clothing [13–22]. This technique provides many benefits to industry with perhaps the most important one being its versatility and simplicity, which means it is a very time efficient way to fabricate a variety of continuous nanofibrous structures. It is advantageous to use the nanofibre webs in a layered structure together with a suited substrate material such that the final product offers sufficient strength and durability. Besides, the nanofibre layers should be flexible and also have a good adherence to the substrates without being easily broken or delaminated [23–25].

In the present study, due to the simplicity of the technique, it is investigated whether electrospinning can also be used to produce nanofibre mat for the efficient shielding of ionizing radiations. In a recent work on WO_3-filled epoxy composites [25], we investigated the effect of nano-sized and micro-sized filler reinforced epoxy composites by melt-mixing method on the X-ray attenuation in the X-ray tube voltage range of 22–127 kV. Our results showed that nano-sized WO_3 was more effective than micro-sized WO_3 in X-ray attenuation at the low X-ray tube range of 22–35 kV since photoelectric interaction dominates at lower photon (X-ray) energy range and also the number of W particles/gram in the nano-sized WO_3-epoxy composite is higher than that for the micro-sized WO_3-epoxy composite. The size effect was not apparent at the higher X-ray tube voltage range of 40–120 kV. Hence, the objective of our present study is to synthesize new radiation shielding materials using the electrospinning technique with the preparation of well-dispersed Bi_2O_3 of different particle sizes in PLA fibre mat. The effectiveness of electrospun nano-Bi_2O_3/PLA nanofibre mats in radiation protection during diagnostic imaging using low X-ray energies is also reported, with the ultimate goal of offering a new approach to radiation protection, based on nanotechnology and electrospinning.

9.2 Results and Discussion

9.2.1 Thickness Measurement

The t_{ave} of all the electrospun Bi_2O_3/PLA nanofibre mats used in Eq. (2.5) is (0.0300 $\pm$ 0.0002) cm which is the chosen constant average thickness of the sample used for the X-ray transmission comparison. On the other hand, t_{ave} of all Bi_2O_3/PLA thin films is (0.0490 $\pm$ 0.0002) cm.

9.2.2 Porosity Measurement

From Table 9.1, the apparent density ρ of each thin film (the last two columns to the right of the table) of the same filler (Bi_2O_3) category increased by the increment of filler content in the PLA solution. The density found in thin films illustrated that m-Bi_2O_3/PLA thin film gives lower density compared to n-Bi_2O_3/PLA thin film but both of them did not make a great difference compared to the theoretical value. However, the apparent density results of the electrospun Bi_2O_3/PLA nanofibre mat underestimated the theoretical values due to the nanofibres were highly porous, randomly oriented and aligned. As can be seen, the density of the electrospun Bi_2O_3/PLA nanofibre mat increased with the filler loading except for the electrospun Bi_2O_3/PLA nanofibre mat of 38 wt% Bi_2O_3 loading; there is a sudden decreased in the density due to the higher porosity found (Table 9.2) and also the formation of PLA beads.

Porosity is an important parameter when preparing the absorbing material for the X-ray attenuation experiment. As can be seen from Table 9.2, the porosity of both electrospun n-Bi_2O_3/PLA nanofibre mat and electrospun m-Bi_2O_3/PLA nanofibre mat was over 70% probably due to the entangled structure of the randomly-oriented nanofibres, indicating that they were highly porous and thus were not really beneficial for the X-ray attenuation by the electrospun nanofibre mat especially with the filler $\geq$38 wt%. Further increases of filler wt% (>38 wt%) was not performed due to the decrease in the sample's density and increasing of the porosity measured

Table 9.1 Density of electrospun Bi_2O_3-PLA nanofibre mats and Bi_2O_3-PLA thin films

Filler (Bi_2O_3) weight fraction (wt%)	Density (cm^3/g)				
	Theoretical	Electrospun nanofibre mat		Thin films	
		Nano	Micro	Nano	Micro
24	1.56	0.27	0.25	1.54	1.50
28	1.63	0.40	0.39	1.59	1.52
34	1.75	0.49	0.45	1.69	1.64
38	1.84	0.30	0.24	1.77	1.72

Table 9.2 Porosity of electrospun Bi_2O_3-PLA nanofibre mats

Filler (Bi_2O_3) weight fraction (wt%)	Porosity (%)	
	Nano-Bi_2O_3 PLA nanofibre mat	Micro-Bi_2O_3 PLA nanofibre mat
0	88.8	88.8
24	83.0	84.0
28	75.4	76.1
34	72.1	74.3
38	83.6	87.0

which can not give any advantages for future X-ray transmission experiments. The porosity found from the control electrospun PLA nanofibre mat was 88.8%. So, if a further investigation was performed for higher filler wt% (>38 wt%), the electrospun Bi_2O_3/PLA nanofibre mat would probably have similar or even higher porosity than this controlled sample.

9.2.3 X-Ray Transmissions

Figure 9.1 shows the XAS X-ray linear attenuation coefficient (μ) results of elec-

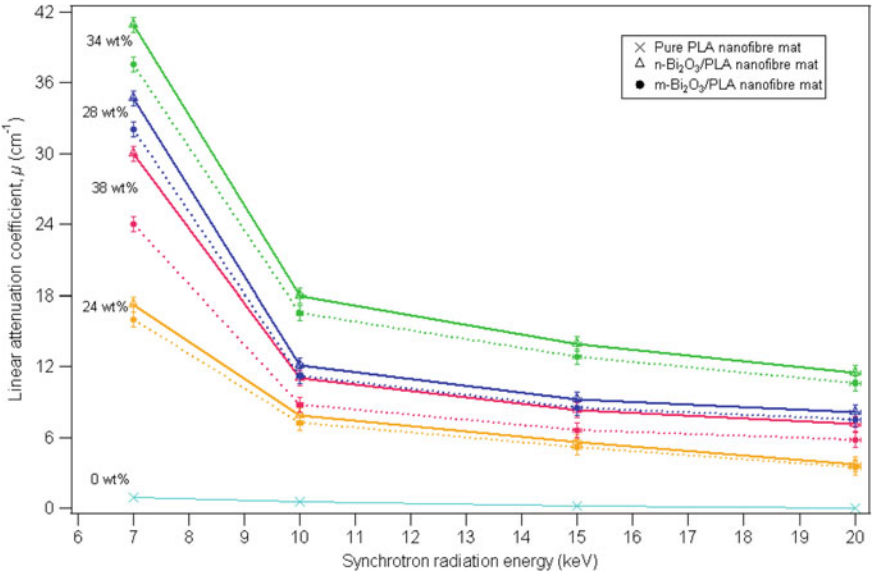

Fig. 9.1 Linear attenuation coefficient as a function of synchrotron radiation energy operated by XAS (7–20 keV) for all Bi_2O_3 loading (0–38 wt%) of the electrospun n-Bi_2O_3/PLA and m-Bi_2O_3/PLA nanofibre mats [28]

trospun nanofibre mats for X-ray energy of 7–20 keV for 0–38 wt% Bi_2O_3 loading. It clearly shows a big difference in T between electrospun n-Bi_2O_3/PLA nanofibre mats and electrospun m-Bi_2O_3/PLA nanofibre mats of the same filler loadings as the X-ray energy increased. Additionally, Fig. 9.2 also shows a distinct difference in μ between electrospun n-Bi_2O_3/PLA nanofibre mats and electrospun m-Bi_2O_3/PLA nanofibre mats at the same filler loadings for the X-ray beams generated by 22–49 kV X-ray tube voltages from the mammography unit. These X-ray tube voltages provided the X-ray effective energy in the range of 15.2–20.8 keV (Fig. 9.3) which were determined using half-value layer (HVL) experiments done by Suk et al. on the mammography unit [26].

As can be seen from both Figs. 9.1 and 9.2, the X-ray μ was reduced with an increase of the filler loading within the PLA matrix for both electrospun n-Bi_2O_3/PLA and m-Bi_2O_3/PLA nanofibre mats except for 38 wt% Bi_2O_3 loading; there is a sudden decrease in X-ray attenuation. These findings support the density and porosity results discussed previously, including the 38 wt% of Bi_2O_3/PLA nanofibre mats which showed low density and high porosity, thus leading to decreased X-ray attenuation. Meanwhile, the comparison of thin-films between m-Bi_2O_3/PLA and n-Bi_2O_3/PLA does not totally support the results found from this study for the electrospun Bi_2O_3/PLA nanofibre mats. As the image in Fig. 9.4 indicate, as the effective X-ray energy increased to >17.4 keV (X-ray tube voltage >35 kV), for the same wt% of Bi_2O_3 filler within this thin film sample, X-ray attenuation for m-Bi_2O_3

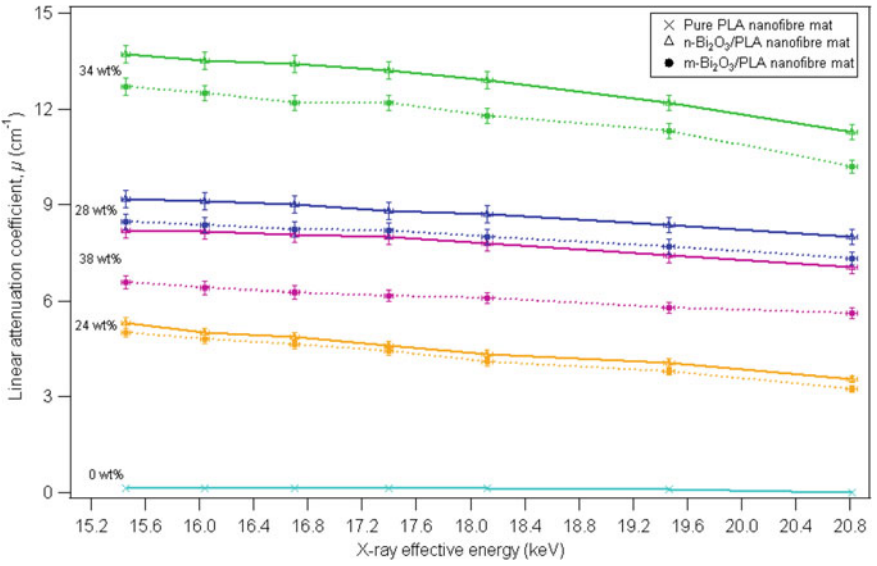

Fig. 9.2 Linear attenuation coefficient as a function of effective energy operated by various X-ray tube voltages of the mammography unit (22–49 kV) for all Bi_2O_3 loading (0–38 wt%) of the electrospun n-Bi_2O_3/PLA and m-Bi_2O_3/PLA nanofibre mats [28]

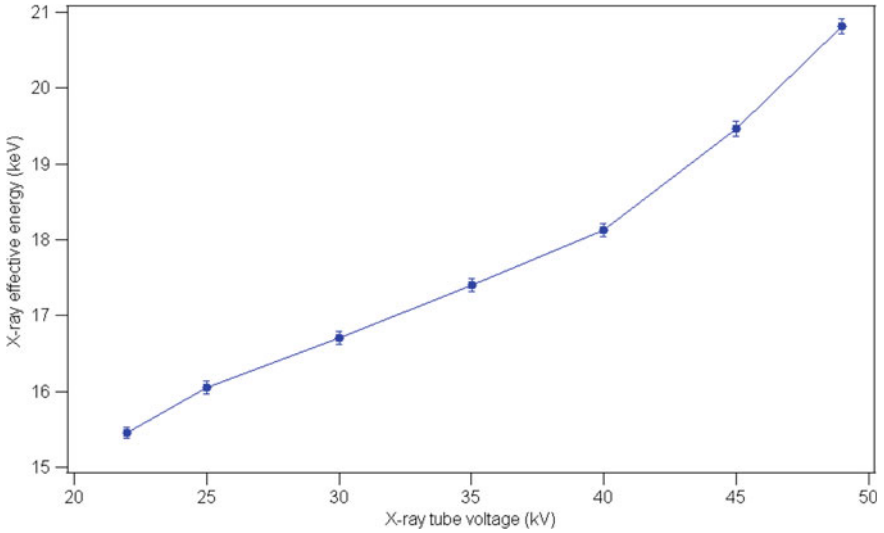

Fig. 9.3 Effective energy as a function of the X-ray tube voltages operated by the mammography unit determined from half-value layer measurements [28]

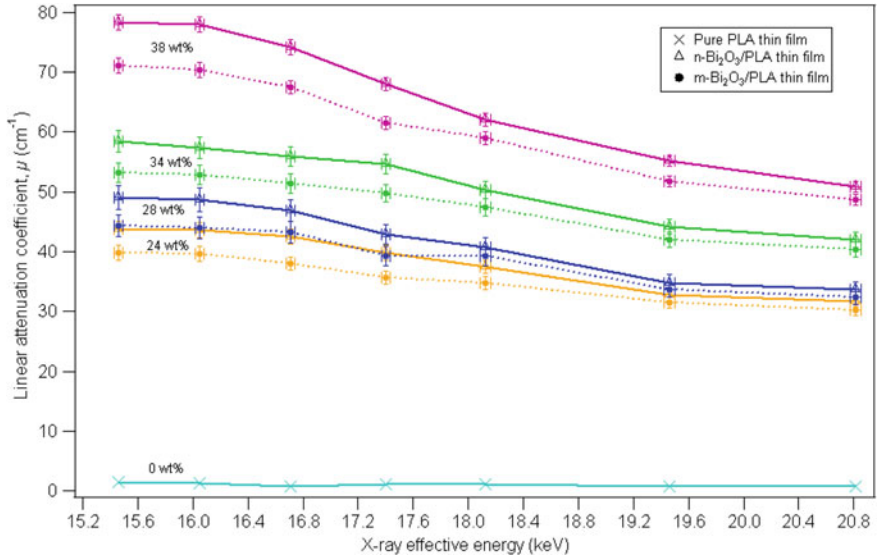

Fig. 9.4 Linear attenuation coefficient as a function of the effective energy operated by various X-ray tube voltages of the mammography unit (22–49 kV) for all Bi_2O_3 loading (0–38 wt%) of the n-Bi_2O_3/PLA and m-Bi_2O_3/PLA thin films [28]

PLA thin film and n-Bi_2O_3/PLA thin film become comparable. They only show significant X-ray attenuation differences for lower X-ray effective energy <17.4 keV (X-ray tube voltage 22–35 kV) operated from the mammography unit.

As in our previous study for the comparison of different sizes of WO_3 particles-epoxy composite [25], we also get similar results for electrospun Bi_2O_3/PLA nanofibre mats which showed that *X-ray attenuation* by electrospun n-Bi_2O_3/PLA nanofibre mat is higher than the *X-ray attenuation* by electrospun m-Bi_2O_3/PLA nanofibre mat with same filler loading (wt%) for lower X-ray tube voltage ranges (22–35 kV) operated from mammography unit. However, by increasing the X-ray tube voltage beyond 35 kV, X-ray attenuation for electrospun n-Bi_2O_3/PLA nanofibre mat is still higher than X-ray attenuation for electrospun m-Bi_2O_3/PLA nanofibre mat. In contrast, in our previous work, the differences in the attenuation by micro-sized WO_3-epoxy composites and nano-sized WO_3-epoxy composites become indistinguishable when the X-ray tube voltage was increased beyond 35 kV [25]. Only Bi_2O_3/PLA thin film has a good agreement with our previous results for X-ray tube voltages greater than 35 kV, which shows the indistinguishability in attenuation between m-Bi_2O_3/PLA thin film and n-Bi_2O_3/PLA thin film.

Figure 9.5 presents the value of μ for electrospun n-Bi_2O_3/PLA nanofibre mats for all the X-ray beam energies generated by XAS and the mammography unit. The results found from XAS unit were correlated with those from the mammography unit since the mammography unit produced effective energies of 15–21 keV with the Mo and Rh anode/filter characteristic X-ray energies of 17.5–22.7 keV, while the X-ray energy used with XAS was ~7–20 keV.

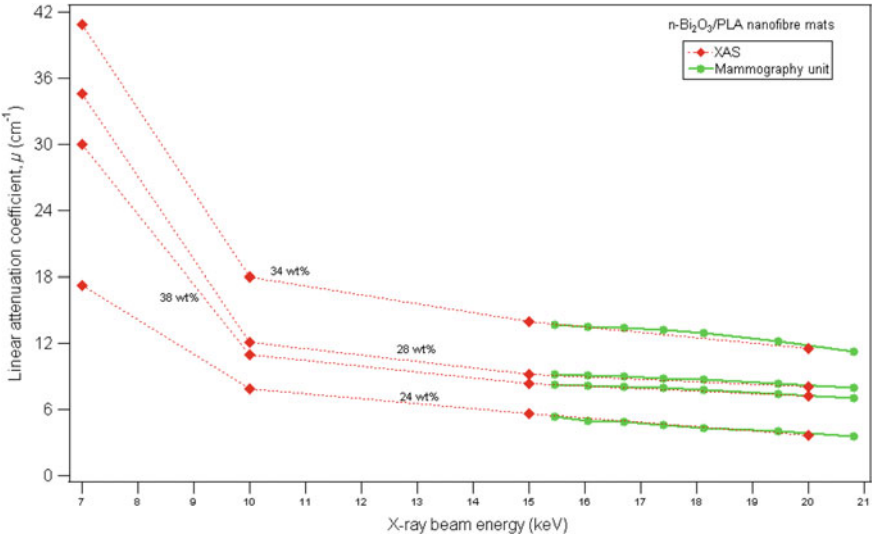

Fig. 9.5 Comparison of the linear attenuation coefficient for the electrospun n-Bi_2O_3/PLA nanofibre mats for all X-ray beam energies generated by XAS and the mammography unit [28]

Therefore, electrospun n-Bi_2O_3/PLA nanofibre mats are superior to their micro-sized counterparts in X-ray attenuation for all the X-ray beam energies (i.e. 7–20 keV and 22–49 kV) generated by XAS and mammography respectively. In contrast, n-Bi_2O_3/PLA thin films are a good X-ray shielding candidate only for the mammography unit of 22–35 kV when compared to m-Bi_2O_3/PLA thin films. Both can be chosen as X-ray shielding materials for X-ray voltages greater than 35 kV.

Basically, the total X-ray attenuation by the absorbing material is determined by three energy-dissipative mechanisms, namely photoelectric effect, Compton scattering and pair production. Pair production was not considered in this study because this mechanism will only occur when the photon energy is beyond 611 keV. In the photoelectric absorption process, a photon undergoes an interaction with an absorber atom in which the photon completely disappears. In its place, an energetic photoelectron is ejected from one of the bound shells of the atom. The photoelectric process is the predominant mode of photon interaction at relatively low photon energies and high atomic number Z, i.e. $(Z/E)^3$. Meanwhile, Compton scattering takes place between the incident photon and one of the outer shell electrons of an atom in the absorbing material. The probability of Compton scattering is almost independent of atomic number Z and X-ray energy E. It is most dominant as the photon energy increases due to a concomitant decrease in the photoelectric effect.

In addition, the number of Bi particles/gram in both n-Bi_2O_3/PLA fibre-mats and thin-films is higher than their micro-sized counterparts. Hence, the probability of X-rays with lowers energies (i.e. 7–20 keV and 22–35 kV) to interact and be absorbed by n-Bi_2O_3 filler is higher when compared to their micro-sized counterparts since the photons interact with the absorbing materials mainly by photoelectric effect.

When the X-ray tube voltage of the mammography unit is more than 35 kV (or characteristic X-ray energy >20 keV), PLA thin-films of n-Bi_2O_3 or m-Bi_2O_3 gave similar X-ray transmission for X-ray tube voltages greater than 35 kV and hence these films can be used for attenuating X-rays generated from these X-ray sources. The observed similarity in the X-ray transmission results may be attributed to: (a) the decrease of the photoelectric effect, and (b) the domination of the Compton scattering effect when the photon (X-ray) energy increases. The latter effect results in less interaction and absorption of the photon by Bi particles of these thin films; thus, the X-ray transmission of these thin films is similar. In contrast, electrospun n-Bi_2O_3/PLA nanofibre mat is superior to their micro-sized counterparts in X-ray attenuation at the same energy range. The observed large differences in X-ray attenuation of these fibre-mats may be explained by the difference in uniformity of dispersion between nano and micro-sized Bi particles within the PLA matrix where large agglomerations tend to occur for the latter.

Hence, the electrospun n-Bi_2O_3/PLA nanofibre mats of all filler loadings (24–38 wt%) are potential candidates in X-ray shielding for all the incident X-ray energy studied either by XAS (7–20 keV) or mammography (22–49 kV) when compared to their micro-sized counterparts. However, the latter may still be a suitable candidate for X-ray shielding of scattered radiations which requires very low energy. These electrospun Bi_2O_3/PLA nanofibre mats can be used as a coating material for X-ray

shielding because PLA nanofibres provide many benefits such as better tenacity, resistance to degradation and mechanical properties [18, 27].

Meanwhile, n-Bi_2O_3/PLA thin films are a good X-ray shielding candidate only for the mammography unit of 25–35 kV when compared to m-Bi_2O_3/PLA thin films. Both can be chosen as the X-ray shielding material for X-ray tube voltage greater than 35 kV.

9.2.4 Microstructure Analyses

The microstructure analysis of the electrospun nanofibres was done using both backscattered electrons and the secondary electrons to clearly show the difference between the PLA polymer and the embedded Bi elements. Figure 9.6a shows the SEM image of control electrospun PLA nanofibres without any Bi_2O_3 filler. The average diameter of these fibres was 854 ± 35 nm. The average diameter of PLA nanofibre increase when 24–34 wt% Bi_2O_3 was added in the PLA solution. For instance, Fig. 9.6b shows the homogenous nanofibres of 28 wt% of n-Bi_2O_3 filler with an average diameter of 971 ± 22 nm. Meanwhile, in Fig. 9.6c the average diameter of 28 wt% m-Bi_2O_3/PLA nanofibres is 911 ± 41 nm with a large variation and agglomerations can be observed.

This indicates that by increasing the solution viscosity while both the conductivity and the surface tension decreased with the increment of filler (Bi_2O_3) loadings within PLA solution, the average nanofibre diameter was increased. The significant increase in the viscosity of solution with increasing filler loadings was due to the increased molecular entanglement which enabled the charged jet to withstand a larger stretching force (from the Coulombic repulsion) resulting in the coarsening of the nanofibres.

In contrast, further increase of Bi_2O_3 loading to 38 wt% caused a decrease in the average diameter to 496 ± 32 nm for n-Bi_2O_3/PLA nanofibres which have a maximum diameter of 2.06 ± 0.49 μm and a minimum of 114 ± 2 nm (Fig. 9.6d). Meanwhile, the average diameter of m-Bi_2O_3/PLA nanofibres is 406 ± 71 nm with a maximum diameter of 1.13 ± 0.23 μm and a minimum of 111 ± 2 nm (Fig. 9.6e). The unexpected decrease in the average fibre diameter may be attributed to the domination of electrical conductivity when filler loading or viscosity of solution increases. As a result, this leads to the production of fibres with non-uniform diameters, as well as formation of beads and particle agglomerations.

Images in Fig. 9.7a–c illustrate the EDS results for the electrospun n-Bi_2O_3/PLA nanofibre mat with 34 wt% filler loading which confirms the existence of Bi element from the filler together with elements C and O from PLA matrix. The SEM images of m-Bi_2O_3/PLA and n-Bi_2O_3/PLA thin films with 28 wt% filler loading are shown in Fig. 9.8 which indicate the presence of agglomerations within PLA matrix.

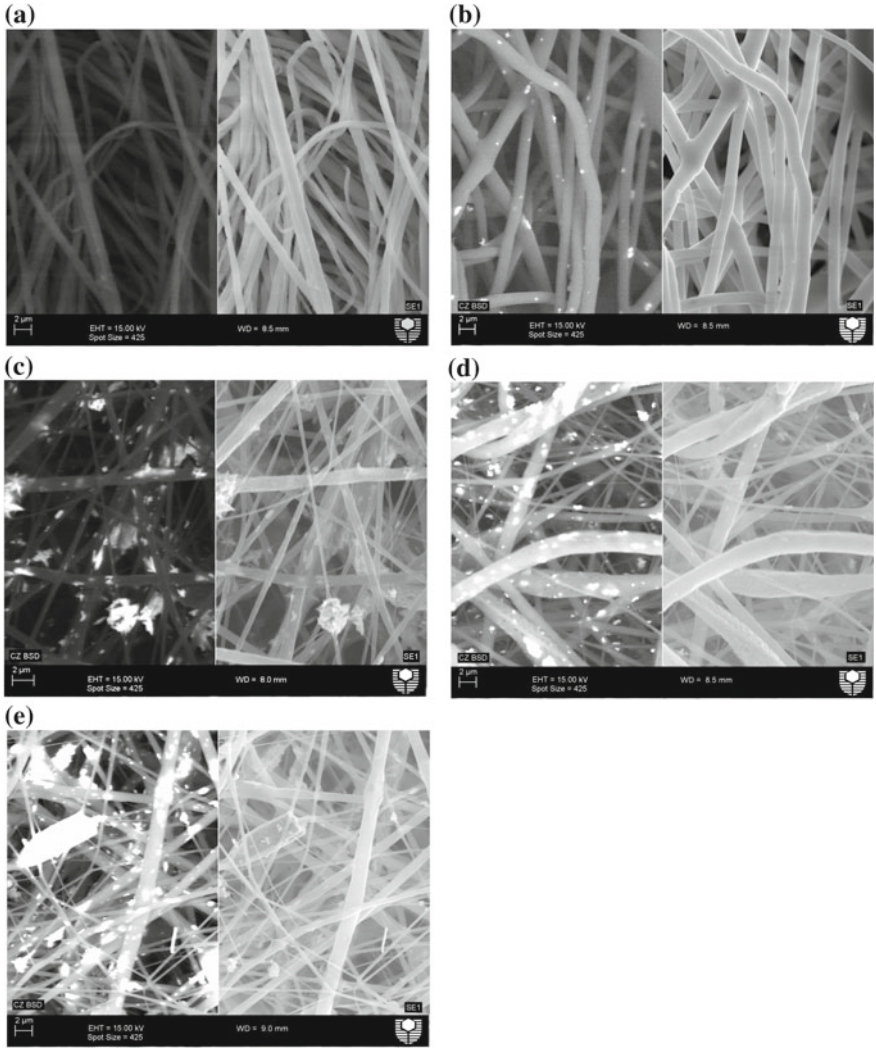

Fig. 9.6 SEM image showing the images performed by backscattered electron technique on the left and the secondary electron technique on the right for **a** the control electrospun PLA nanofibres without any particles (0 wt% of Bi_2O_3); **b** 28 wt% Bi_2O_3 of electrospun n-Bi_2O_3/PLA nanofibres; **c** 28 wt% Bi_2O_3 of electrospun m-Bi_2O_3/PLA nanofibres; **d** 38 wt% Bi_2O_3 of electrospun n-Bi_2O_3/PLA nanofibres; and **e** 38 wt% Bi_2O_3 of electrospun m-Bi_2O_3/PLA nanofibers [28]

9.3 Conclusions

The electrospun nanofibre mats of n-Bi_2O_3/PLA and m-Bi_2O_3/PLA with filler loadings of 24–38 wt% were successfully fabricated. From the analyses, the electrospun n-Bi_2O_3/PLA nanofibre mats of all filler loadings are superior in attenuating X-rays

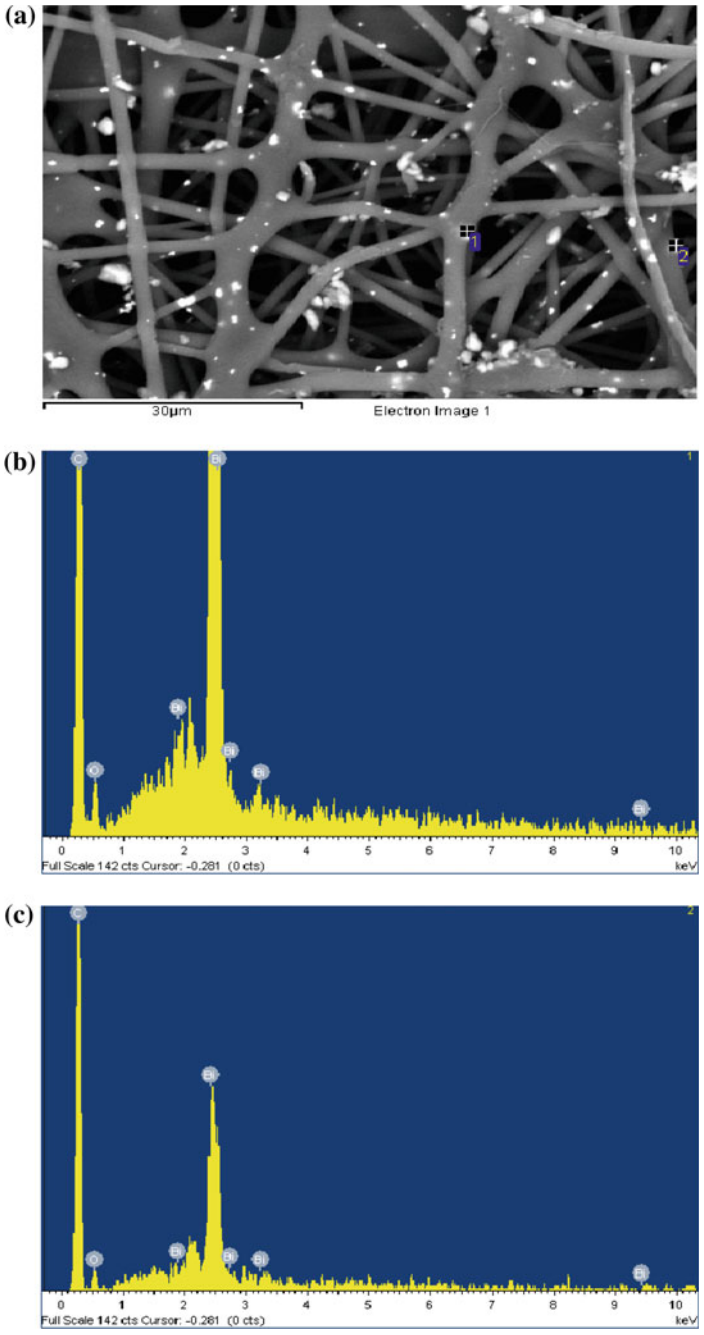

Fig. 9.7 **a** SEM image used for EDS analyses on 34 wt% Bi_2O_3 of the electrospun n-Bi_2O_3/PLA nanofibres to prove that only Bi particles detected other than C and O which is the composition of PLA; EDS analyses for **b** point 1 and; **c** point 2 marked in **a** [28]

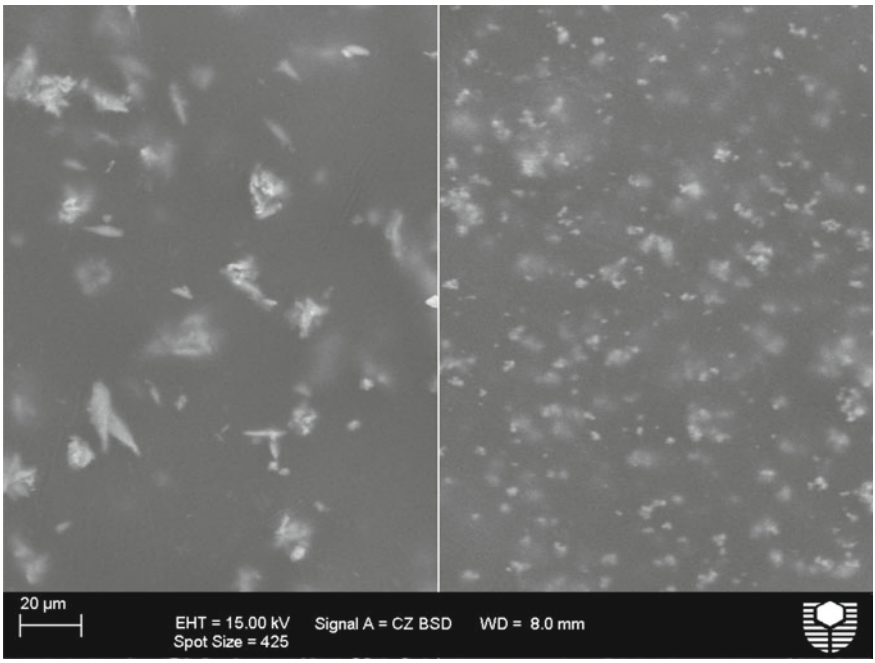

Fig. 9.8 SEM images of the thin film of 28 wt% Bi_2O_3 for m-Bi_2O_3/PLA on the left showing agglomerations and n-Bi_2O_3/PLA on the right [28]

as compared to their micro-sized counterparts because the X-ray transmission is strongly dependent on the particle size and the photoelectric interaction. However, the electrospun Bi_2O_3/PLA nanofibre mats with 38 wt% loading is not recommended for X-ray shielding because of higher porosity as compared to the lower filler loadings. The n-Bi_2O_3/PLA thin films are a good X-ray shielding candidate only for the mammography unit of 22–35 kV when compared to the m-Bi_2O_3/PLA thin films. The particle size effect on X-ray attenuation diminished as the X-ray tube voltage exceeds 35 kV.

Acknowledgements The collection of X-ray absorption spectroscopy (XAS) data was funded by the Australian Synchrotron (AS123/XAS5341). We thank our colleagues Dr. C. Ng and A/Prof. Z. Sun for assistance with XAS data collection. Also, we would like to thank Carolyn Madeley of Breast Assessment Centre, Royal Perth Hospital, Western Australia for giving us the opportunity to use the mammography unit.

References

1. Patra CR, Bhattacharya R, Mukhopadhyay D, Mukherjee P (2010) Fabrication of gold nanoparticles for targeted therapy in pancreatic cancer. Adv Drug Deliv Rev 62:346–361
2. Huang X, El-Sayed MA (2010) Gold nanoparticles: optical properties and implementations in cancer diagnosis and photothermal therapy. J Adv Res 1:13–28
3. Granmayeh Rad A, Abbasi H, Afzali MH (2011) Gold nanoparticles: Optical properties and implementations in cancer diagnosis and photothermal therapy. Phys Procedia 22:203–208
4. Sahare PD, Ranju R, Numan S, Lochab SP (2007) K3Na(SO4)2: Eu nanoparticles for high dose of ionizing radiation. J Phys D Appl Phys 40:759
5. Lines MG (2008) Nanomaterials for practical functional uses. J Alloy Compd 449:242–245
6. Haiwen X, Kai-Zhong G, Yiming S, Song X (2006) Precessional dynamics of single domain magnetic nanoparticles driven by small ac magnetic fields. J Phys D Appl Phys 39:4746
7. Popov A (2009) Sun protection using nanoparticles 24:1–2
8. Storrie H, Mooney DJ (2006) Sustained delivery of plasmid DNA from polymeric scaffolds for tissue engineering. Adv Drug Deliv Rev 58:500–514
9. Botelho MZ, Künzel R, Okuno E, Levenhagen RS, Basegio T, Bergmann CP (2011) X-ray transmission through nanostructured and microstructured CuO materials. Appl Radiat Isot 69:527–530
10. El Haber F, Froyer G (2008) Transparent polymers embedding nanoparticles for x-rays attenuation (Review). J Univ Chem Technol Metall 43:283–290
11. Buyuk B, Tugrul AB, Akarsu AC, Addemir AO (2012) Investigation on the effects of titanium diboride particle size on radiation shielding properties of titanium diboride reinforced boron carbide-silicon carbide composites'. J Nano- Electron Phys 4:01010(01011)–01010(01014)
12. Künzel R, Okuno E (2012) Effects of the particle sizes and concentrations on the X-ray absorption by CuO compounds. Appl Radiat Isot 70:781–784
13. Faccini M, Vaquero C, Amantia D (2012) Development of protective clothing against nanoparticle based on electrospun nanofibres. J Nanomater 2012:1–9
14. Molamma PP, Venugopal J, Casey KC, Ramakrishna S (2008) Surface modified electrospun nanofibrous scaffolds for nerve tissue engineering. Nanotechnology 19:455102
15. Sill TJ, von Recum HA (2008) Electrospinning: Applications in drug delivery and tissue engineering', Biomaterials 29:1989–2006
16. Russo G, Lamberti G (2011) Electrospinning of drug-loaded polymer systems: Preparation and drug release. J Appl Polym Sci 122:3551–3556
17. Huang S, Kang X, Cheng Z, Ma P, Jia Y, Lin J (2012) Electrospinning preparation and drug delivery properties of Eu3+/Tb3+ doped mesoporous bioactive glass nanofibres. J Colloid Interface Sci 387:285–291
18. Haroosh HJ, Chaudhary DS, Dong Y (2012) Electrospun PLA/PCL fibres with tubular nanoclay: Morphological and structural analysis. J Appl Polym Sci 124:3930–3939
19. Yiin-Kuen F, Li-Chih L (2013) Pattern transfer of aligned metal nano/microwires as flexible transparent electrodes using an electrospun nanofiber template. Nanotechnology 24:055301
20. Rajeswari R, Jayarama Reddy V, Subramanian S, Shayanti M, Radhakrishnan S, Seeram R (2012) Minimally invasive injectable short nanofibres of poly(glycerol sebacate) for cardiac tissue engineering. Nanotechnology 23:385102
21. Hu W, Huang ZM, Liu XY (2010) Development of braided drug-loaded nanofibre sutures. Nanotechnology 21:315104
22. Yu DG, Shen XX, Chris BW, Kenneth W, Zhu LM, Bligh SWA (2009) Oral fast dissolving drug delivery membranes prepared from electrospun polyvinylpyrrolidone ultrafine fibres. Nanotechnology 20:055104
23. Lee S, Obendorf SK (2007) Use of electrospun nanofibre web for protective textile materials as barriers to liquid penetration. Text Res J 77:696–702
24. Brettmann BK, Tsang S, Forward KM, Rutledge GC, Myerson AS, Trout BL (2012) Free surface electrospinning of fibres containing microparticles. Langmuir 28:9714–9721

25. Noor Azman NZ, Siddiqui SA, Hart R, Low IM (2013) Effect of particle size, filler loadings and x-ray tube voltage on the transmitted x-ray transmission in tungsten oxide-epoxy composites. Appl Radiat Isot 71:62–67
26. Suk CC, Wei LJ, Harun AZ (2012) Evaluation of X-ray beam quality based on measurements and estimations using SpekCalc and Ipem78 models', Malays J Med Sci 19:22–28
27. Farrington DW, Lunt J, Davies S, Blackburn RS (2005) Biodegradable and sustainable fibres', in Poly (lactic acid) fibres. Woodhead Publishing Series in Textiles, Cambridge, United Kingdom, pp 191–220
28. Noor Azman NZ, Siddiqui SA, Haroosh HJ, Albetran HM, Johannessen B, Dong Y, Low IM (2013) oxide/polylactic acid nanofibre mats. J Synchrotron Radiat 20:741–748